J Eng Math (2008) 60:115–124
DOI 10.1007/s10665-007-9150-x

An efficient numerical method for highly loaded transonic cascade flow

Yi Liu

Received: 7 April 2006 / Accepted: 4 May 2007 / Published online: 3 August 2007

Abstract In this paper, an efficient numerical method for transonic viscous flow in a highly loaded turbine vane cascade, where the interaction of a shock wave and boundary layer often leads to very complicated flow phenomena, is developed. The numerical code, a modified implicit flux-vector-splitting solver of the Navier–Stokes equations (MIFVS), is extended to simulate such transonic cascade flow. A compressible low-Reynolds-number k–ε model, together with a transition-modified damping function, has been implemented into the MIFVS code. With this extended MIFVS solver, the main feature of transonic flow and shock and boundary-layer interactions in the highly loaded transonic turbine vane are efficiently predicted with satisfactory accuracy. The convergence rate is found to be three times faster than that of flux-vector-splitting (FVS) methods.

Keywords Boundary layer · Highly loaded · Implicit · Shock · Transonic turbine flow

1 Introduction

Turbine blades are thought to be state-of-the-art in terms of their loading and design philosophy through a sustainable development of advanced computational fluid dynamics (CFD) methodologies and the experimental approaches available at the present time. In recent years, efforts have been directed towards designing blades with increasing aerodynamic loading (lift coefficient), leading to the so-called high-lift profiles [1–6]. The large pressure ratio and high loading coefficient in such turbine blades could lead to a complicated transonic flow pattern with shock waves and separated zones, especially in blades with large blade-turning angles and high exit Mach numbers.

The aerodynamic efficiency and loading coefficient of highly loaded turbine blades need to be carefully optimized. If no separation occurs on the blade surface and the blade aerodynamic loading distribution is properly controlled, highly loaded blade can offer higher efficiency and lower cost when compared with conventional blades. On the other hand, if separation does occur, their performance can be considerably worse than that of conventional blades. Therefore, special attention should be paid to the design and analysis of highly loaded blades. A key numerical challenge is to accurately model the flow features while maintaining a high numerical efficiency.

In this paper, a well-established numerical code, the modified implicit flux-vector-splitting solver (MIFVS) [7–9], is employed to investigate such transonic flow in a highly loaded VKI turbine guide-vane cascade [10,11].

Y. Liu (✉)
Department of Engineering Science, University of Oxford, Oxford OX2 0EP, UK
e-mail: yi.liu@eng.ox.ac.uk

This code has been developed and applied to various other flows, with many advantages in terms of accuracy, convergence and computing cost [7,9,12,13]. New challenges in the present code development require accurate turbulence and transition models to be incorporated into the MIFVS. The approaches and methodologies to achieve these code improvements are presented and discussed. The performance of the extended MIFVS method is assessed by extensive comparisons with the experimental and available computed results for a transonic highly loaded turbine blade.

2 Governing equations

2.1 Navier–Stokes equations

The continuity, momentum and energy conservation equations of the Reynolds averaged Navier–Stokes (RANS) equations can be written in terms of generalized coordinates and in a conservative flux-vector-splitting form as follows

$$\frac{\partial \hat{\mathbf{U}}}{\partial \tau} + \frac{\partial \hat{\mathbf{F}}_i^+}{\partial \xi_i} + \frac{\partial \hat{\mathbf{F}}_i^-}{\partial \xi_i} + \mathbf{S}_1 = \frac{1}{\mathrm{Re}} \left[\frac{\partial \hat{\mathbf{F}}\mathbf{v}_i}{\partial \xi_i} + \mathbf{S}_2 \right], \tag{1}$$

where τ, ξ_i are the independent variable for time and general curvilinear coordinates in the grid domain, $\hat{\mathbf{U}}$ is the conservative flow-variable vector $[\rho,\ \rho u_i,\ \rho E]^{\mathrm{T}}$, $\hat{\mathbf{F}}_i^{\pm}$, $\hat{\mathbf{F}}\mathbf{v}_i$ are the inviscid splitting and viscous flux vectors in generalized coordinates, and $\hat{\mathbf{S}}_1$, $\hat{\mathbf{S}}_2$ are the source terms, which are distinctly different in nature: one is caused by the convection term encountered in cylindrical coordinates and considering rotation effects, and the other exists due to the diffusion term. References [7,13] present detailed elements of each term as applied in the MIFVS code.

2.2 Low-Reynolds-number k–ε model

The Chien formulation of the low-Reynolds number k–ε turbulence model [14] uses the turbulent kinetic energy k and the dissipation rate ε as the principal variables. In this study, we apply this model, with Sarkar's compressibility modification [15], into the MIFVS code to simulate the turbulent boundary layer and its interaction with shock waves. The governing equations can be cast in the same form as the RANS equations (Eq. 1)

$$\frac{\partial \hat{\mathbf{U}}^{k\varepsilon}}{\partial \tau} + \frac{\partial (\hat{\mathbf{F}}_i^+)^{k\varepsilon}}{\partial \xi_i} + \frac{\partial (\hat{\mathbf{F}}_i^-)^{k\varepsilon}}{\partial \xi_i} + \mathbf{S}_1^{k\varepsilon} = \frac{1}{\mathrm{Re}} \left[\frac{\partial (\hat{\mathbf{F}}\mathbf{v}_i)^{k\varepsilon}}{\partial \xi_i} + \mathbf{S}_2^{k\varepsilon} \right]. \tag{2}$$

The similarities between Eqs. 1 and 2 make it straightforward to extend the method of implicit formulation and eigenvalue analysis of RANS equations to the turbulence-model solver. The flux and source terms of Eq. 2 are

$$\hat{\mathbf{U}}^{k\varepsilon} = \mathrm{J} \begin{pmatrix} \rho k \\ \rho \bar{\varepsilon} \end{pmatrix}, \quad (\hat{\mathbf{F}}_i^{\pm})^{k\varepsilon} = J \begin{pmatrix} \rho k \hat{U}_i^{\pm} \\ \rho \bar{\varepsilon} \hat{U}_i^{\pm} \end{pmatrix}, \quad (\hat{\mathbf{F}}\mathbf{v}_i)^{k\varepsilon} = J \begin{pmatrix} \left(\mu + \dfrac{\mu_t}{\sigma_k}\right) \dfrac{\partial k}{\partial x_i} \\ \left(\mu + \dfrac{\mu_t}{\sigma_\varepsilon}\right) \dfrac{\partial \bar{\varepsilon}}{\partial x_i} \end{pmatrix},$$

$$\hat{\mathbf{S}}_2^{k\varepsilon} = J \begin{pmatrix} P_k - \rho(1+\Gamma)\bar{\varepsilon} \\ C_{\varepsilon 1} f_1 P_k \dfrac{\bar{\varepsilon}}{k} - C_{\varepsilon 2} f_2 \rho \dfrac{\bar{\varepsilon}^2}{k} + 2\nu\rho \dfrac{\bar{\varepsilon}}{Y^2} \exp(-0.5Y) \end{pmatrix},$$

$$\mu_t = C_\mu f_\mu \frac{\rho k^2}{\varepsilon}, \qquad \bar{\varepsilon} = \varepsilon + 2\nu \frac{k}{y^2}, \qquad P_k = \tau_{ij}^{\mathrm{turb}} \frac{\partial u_i}{\partial x_j},$$

where Γ is compressibility correction function. Several correction functions have been developed by different authors. The widely used compressibility modification proposed by Sarkar et al. [15], among other correction functions, is employed in this study;

$$\Gamma = \mathrm{Ma}_T^2 \qquad \text{with } \mathrm{Ma}_T = \frac{\sqrt{k/\rho}}{a}.$$

The damping functions and model constants are:

$$f_\mu = 1 - \exp(-0.0115 y^+),$$

$$f_1 = 1, \quad f_2 = 1 - 0.22 \exp[1 - (\mathrm{Re}_{t/6})^2], \tag{3}$$

$$\mathrm{Re}_t = \frac{\rho k^2}{\mu \bar{\varepsilon}}, \quad \mathrm{Re}_y = \frac{\rho \sqrt{k} y}{\mu}, \quad y^+ = \frac{y \rho U^*}{\mu}, \quad U^* = \sqrt{\frac{\tau_w}{\rho}},$$
$$C_\mu = 0.09, \quad C_{\varepsilon 1} = 1.35, \quad C_{\varepsilon 2} = 1.80, \quad \sigma_k = 1.0, \quad \sigma_\varepsilon = 1.3.$$

2.3 Transition model

Transition to turbulence and re-laminarization may both occur in turbine cascade flows and are strongly affected by large pressure gradients, positive and/or negative. In the transonic highly loaded turbine blade, the trailing-edge shock departing from the pressure surface, and possibly the internal shock originating from the suction surface, impinges on the opposite surface of the adjoining blade, thereby interacting with the boundary layer. The impinging shock thickens the boundary layer, causing total pressure losses to be increased, when the boundary layer is turbulent. If the boundary layer is laminar, the flow can separate and transition takes place in the separated shear layer or near the reattachment point. The transition model embodied in the low-Reynolds-number k–ε turbulent model is described here.

The damping function of Eq. 3, f_μ, is modified to include the ratio $25/A^+$ [16], which represents an intermittency function

$$f_\mu = 1 - \exp\left(-0.0115 y^+ \frac{25}{A^+}\right). \tag{4}$$

The parameter A^+ is set a critical value (300) in laminar flows to guarantee the turbulence viscosity, μ_t, very small. The normal expression of f_μ (Eq. 3) is restored for fully turbulent boundary layer when A^+ equals 25. In the transition region, A^+ is interpolated according to the local value of the momentum thickness Reynolds number.

2.4 Leading-edge correction

Most k–ε turbulence models are found to predict excessive levels of turbulent energy in stagnation regions, as often shown in the blunt leading edge of highly loaded transonic turbine blades [17]. In these regions, the Boussinesq assumption fails in flows with large normal strain and this results in excessive production of turbulent energy in stagnation flows. When convected downstream these disturbances can influence the entire boundary layer significantly, which is why the reformulated expression for production term proposed by Kato and Launder [18] is considered.

Bypassing the eddy-viscosity relation for the Reynolds stresses allows the production term P_k to be modified:

$$P_k = \mu_t S \Omega, \quad S = \sqrt{2\left(\frac{\partial u_i}{\partial x_j} + \frac{\partial u_j}{\partial x_i}\right)}, \quad \Omega = \sqrt{2\left(\frac{\partial u_i}{\partial x_j} - \frac{\partial u_j}{\partial x_i}\right)},$$

where Ω is the rotation parameter which is proportional to the magnitude of the local vorticity. The flow does not have any vorticity on the stagnation streamline; hence $\Omega = 0$ there. On the other hand, in simple shear layers the corrected production term, P_k, is identical to the standard one, and thus the constants of the k–ε model do not need to be recalibrated for this correction.

3 Computational methods

3.1 Implicit formulation

An implicit formulation for the NS equations has been developed which uses the spectral-radii technique to simplify the calculation and at the same time avoids the approximate factorization [19] to increase the time step and stability.

The semi-discrete delta expression for Eq. 1 also applicable to (2) of the low-Reynolds-number k–ε model, is derived as in [7,8]

$$\begin{aligned}\delta\mathbf{U}^{n+1} &= \Delta\mathbf{U}^{n} + \Delta t\left\{-\sum_{i=1}^{3}\frac{\partial(\lambda_{Ii}^{+}\delta\mathbf{U}^{n+1}+\lambda_{Ii}^{-}\delta\mathbf{U}^{n+1})}{\partial\xi_i} - \lambda_{1S}\delta\mathbf{U}^{n+1} + \sum_{i=1}^{3}\frac{\partial^2(\lambda_{vi}\delta\mathbf{U}^{n+1})}{\partial\xi_i^2}\right.\\ &\quad\left.+\sum_{i=1}^{3}\frac{\partial(\lambda_{Si}^{+}\delta\mathbf{U}^{n+1}+\lambda_{Si}^{-}\delta\mathbf{U}^{n+1})}{\partial\xi_i}\right\},\\ \mathbf{U}^{n+1} &= \mathbf{U}^{n}+\delta\mathbf{U}^{n+1}.\end{aligned} \tag{5}$$

3.2 Spatial discretisation

The upwind scheme is utilized to calculate the explicit part of (5) through the Steger–Warming technique of flux-vector splitting (FVS) [20]:

$$\Delta\mathbf{U}^{n} = -\Delta t\left[\sum_{i=1,3}\left(\frac{\nabla\mathbf{F}_i^{+}}{\Delta\xi_i}+\frac{\Delta\mathbf{F}_i^{-}}{\Delta\xi_i}\right)+\mathbf{S}_1-\frac{1}{\mathrm{Re}}\left(\sum_{i=1,3}\frac{\Delta_c\mathbf{F}\mathbf{v}_i}{\Delta\xi_i}+\mathbf{S}_2\right)\right]^{n}.$$

It has been demonstrated that the current implicit formulation is adequately efficient when applied to FVS methods, while maintaining a high level of robustness and accuracy [7–9,12].

Compared with conventional implicit methods, the MIFVS is a Jacobian spectral-radius scheme and a non-approximate-factorization scheme. There is no second-order dissipation in any form and no artificial viscosity. The transonic cascade flow in the highly loaded turbine blades is thus solved by extending the MIFVS solver to include the transition-modified low-Reynolds-number k–ε turbulence model.

3.3 Computational grid

For an accurate representation of the flow field, multi-block topology is employed to generate a better-quality grid for highly loaded turbine blades with large turning angles and a blunt leading/trailing edge. Various grid densities and nodal distributions have been used to study the influence of the discretization on the physical domain.

Figure 1 shows a typical periodic cascade H-mesh grid (every other point), in which the blade is embodied in the computational domain. The periodic boundary is preserved by the nodal periodic distributions. The grid, based on a periodic O-mesh in which the orthogonal meshing is implemented around the blade, patched with an outlet periodic H-mesh, is also generated (not shown here). The numerical simulations show that the periodic O-mesh obtained slightly better results near the trailing edge when vortex shedding exists in the high exit-Mach-number calculations (as shown in Fig. 3). In other regimes, they both show almost identical results.

A specific distribution along the pitch direction, as shown in Fig. 2, a smoother combination of linear and logarithm functions is accomplished to refine the mesh near the wall to improve boundary layer resolution. The first grid point away from the blade is placed at a y^{+} of about 1–20, with approximately 20 points within the boundary layer. The nodal distributions are gradually relaxed towards the inlet and outlet boundaries.

Note that all the grids have improved smoothness and orthogonality by solving the Poisson equations using initial grids generated algebraically. As a result, the grid distribution function plotted in Fig. 2 is not necessarily symmetric.

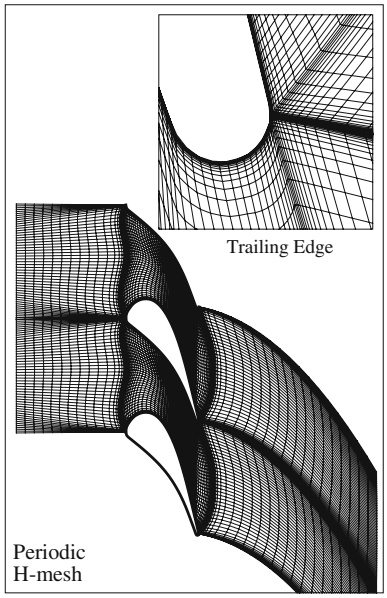

Fig. 1 Computational domain and grid

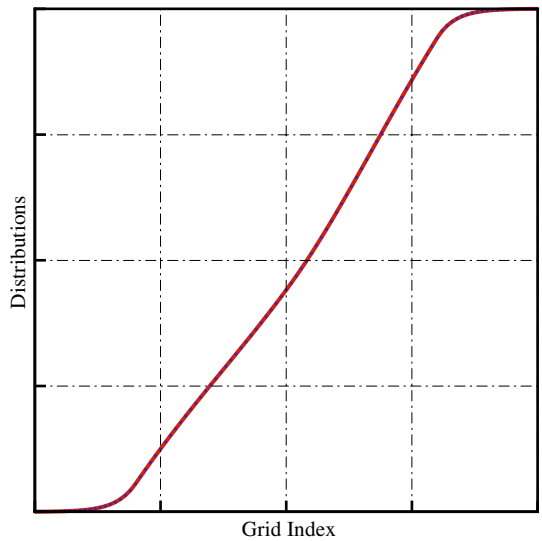

Fig. 2 The grid distributions along pitch direction

3.4 Boundary conditions

The boundary conditions for turbine cascade simulations include inflow, outflow, solid walls and geometrical periodic boundaries. The total pressure and total temperature, together with the flow directions, are specified in the inflow boundary. The turbulence intensity and length scale are prescribed in order to determine the turbulent kinetic energy and dissipation of kinetic energy, respectively. Two outflow boundary conditions are available: the exit pressure distribution for subsonic flows and extrapolation for supersonic flows. On solid walls, rigid impermeable non-slip is specified. Finally, the periodic boundaries between the blades are solved in the same manner as interior cells by extending a row of dummy grid cells.

4 Results and discussion

A highly loaded transonic turbine-nozzle guide vane (NGV), tested by Arts [10,11], has been simulated. The NGV has been widely accepted as a numerical validation case, since there are a wealth of experimental data available over a wide range of the exit Mach number, $M_{2,\mathrm{is}}$, the exit Reynolds number, Re_2, the inlet turbulence intensity, Tu, and the gas to the wall-temperature ratio, *etc*.

The flow field is initialized with uniform conditions corresponding to an inlet Mach number of 0.15. Although it is beneficial to start with a low exit-Mach-number flow field, there was little problem with regard to convergence with the MIFVS. The typical convergence history is shown in Fig. 3. In comparison, the simulation with the commercially available code, `Fluent` [21], exhibits a slow convergent trend (>12,000 time steps). It demonstrates the present implicit accelerating method has the striking efficiency to solve the viscous flow over the highly loaded turbine blades (<5,000 time steps). With implicit acceleration, it gives at least three times as fast a convergence rate as the FVS solver. This observation is consistent with numerical experiments with other applications [8,12,13].

Note that the monitor parameter near the blunt trailing edge shows the occurrence of periodic vortex shedding, even in the current steady nature of the calculation.

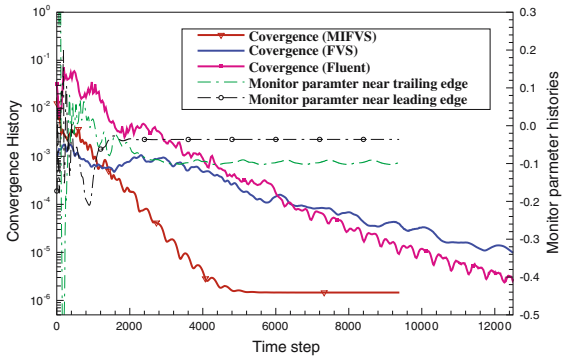

Fig. 3 The monitored convergence histories

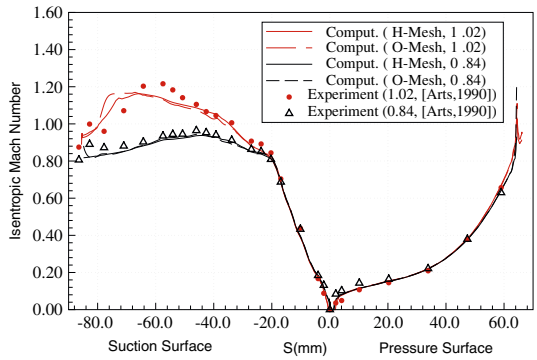

Fig. 4 The isentropic Mach number distributions along blade surfaces

Figure 4 shows calculated and measured isentropic Mach number (M_{is}) distributions along the vane surface, for the exit Mach numbers ($M_{2,is}$) of 0.85 and 1.02, respectively. The measurements and simulations were performed with an exit Reynolds number of 10^6. In the $M_{2,is} = 0.85$ case, the flow is observed to steeply accelerate along the suction side up to about 20 mm, then a weak recompression is followed by a re-acceleration. The Mach number distribution is then rather flat with a slightly adverse pressure gradient starting from approximately 50 mm. The velocity distribution along the pressure surface varies smoothly downstream of the leading edge. Both H-type and O-type grids yield similar distributions, except near the trailing edge. In general, the agreements with experimental data are satisfactory.

For the $M_{2,is} = 1.02$ case, the Mach number distribution along the pressure surface is almost the same as that in the $M_{2,is} = 0.85$ case. The flow again steeply accelerates along the suction side up to 20 mm, then accelerates at slowly reducing rates up to a high peak Mach number of nearly 1.2. The adverse pressure gradients do not appear until at a location of about 40 mm. However, the simulations by both grids fail to accurately capture the location of the peak Mach number (about 10% lower). This is probably due to the employed turbulence model or grid resolution at the rear of the blade.

Computed wake profiles located at 43.3% of axial chord downstream of the trailing edge are compared to the experimental data, digitized manually from [10], in Fig. 5. Here, again we see a better agreement in the $M_{2,is} = 0.85$ case.

To visualize the transonic flow pattern and shock/boundary-layer interaction, in Fig. 6, the numerical Schlieren (contours of density-gradient magnitude) for the $M_{2,is} = 1.02$ case is elucidated. This is comparable with the experimental Schlieren photograph [10]. A normal shock is observed along the rear part of the suction side at the location of about 60 mm. The calculation is consistent with the Schlieren picture in terms of shock location and inclination. The weak trailing-edge shock departing from the pressure side is also well captured.

The good agreement in the surface Mach number distributions (Fig. 4), the wake profiles (Fig. 5) and the flow structure (Fig. 6) with the experimental data validates the extended MIFVS code, and allows us to numerically investigate the details of transonic cascade-flow features with confidence. Further simulated results are presented in Fig. 7, in the form of Mach number and nondimensional static pressure contours. The flow characteristics, such as shock and its interactions with wake and boundary layer, are clearly seen.

The shock and its interactions with wake and boundary layer becomes stronger for a high exit Mach number, consequently separation can occur. Figure 8 shows the axial velocity contours and velocity vectors. It corresponds to an isentropic Mach number of $M_{2,is} = 1.10$, an exit Reynolds number of $Re_2 = 5 \times 10^5$ and a free stream turbulence intensity of Tu = 6%, which presents a stronger shock wave on the suction side just before the trailing edge. Unlike the $M_{2,is} = 1.02$ case, this trailing-edge shock, issuing from the pressure side, impinges on the suction surface (marked in Fig. 8a), interacts with a laminar boundary layer and causes the flow separation. This is further

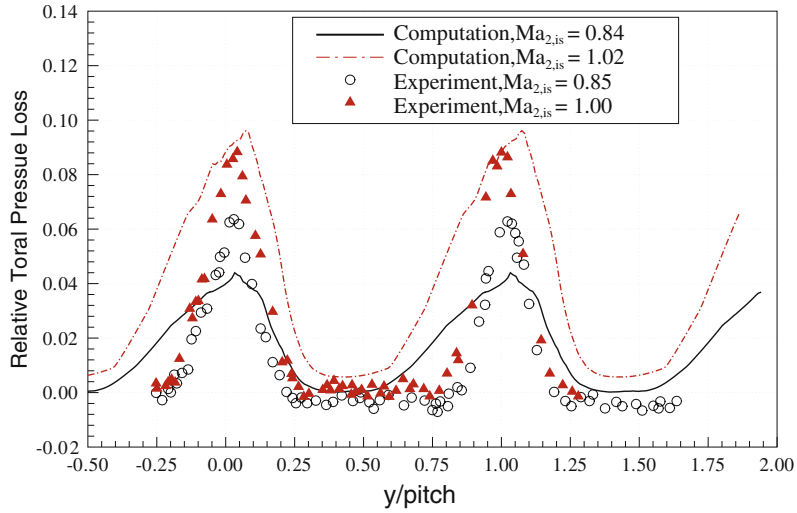

Fig. 5 The wake profiles of the total pressure

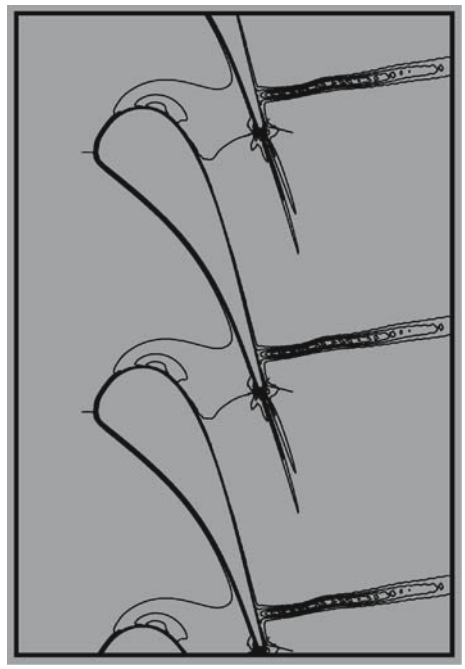

Fig. 6 Simulated contours of density-gradient magnitude (numerical Schlieren) for the $M_{2,\mathrm{is}} = 1.02$ case

illustrated by the velocity vectors of Fig. 8b. As a consequence, the trailing-edge shock moves forward, and is not right at the trailing edge as in the inviscid simulation.

Similar to the $M_{2,\mathrm{is}} = 1.02$ case, we generate the numerical Schlieren for a high exit Mach number of 1.10 case in Fig. 9. The acceleration is stronger and the boundary layer on the suction side remains laminar over a large part of the blade. A normal shock is moved further downstream of the suction side. Consistent with Fig. 8a, the trailing edge shock is clearly seen.

By simulating such complex flows, the MIFVS method demonstrates the ability of solving flow in the highly loaded turbine-vane cascade. The computed results show that the present solution procedure is able to predict the main flow feature with good agreement with the experimental data and published numerical results.

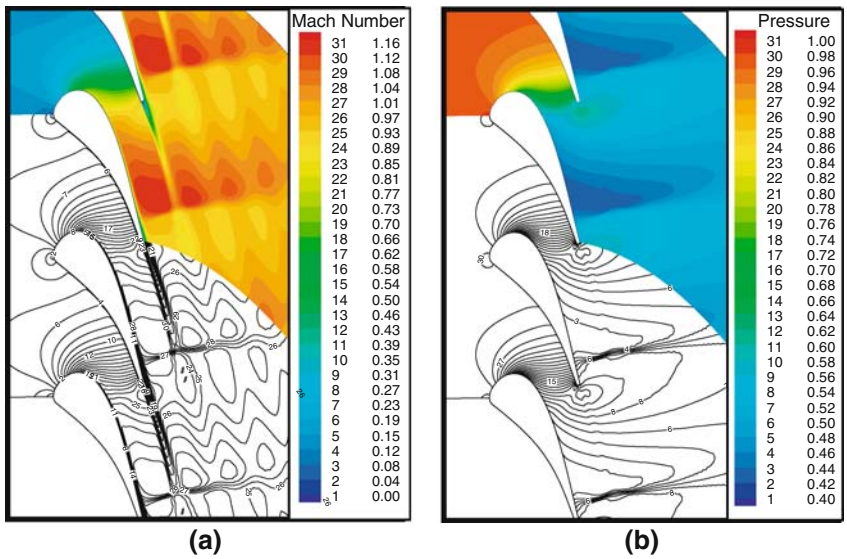

Fig. 7 Simulated contour plots of Mach number (**a**), nondimensional static pressure pressure (**b**) for the $M_{2,\mathrm{is}} = 1.02$ case

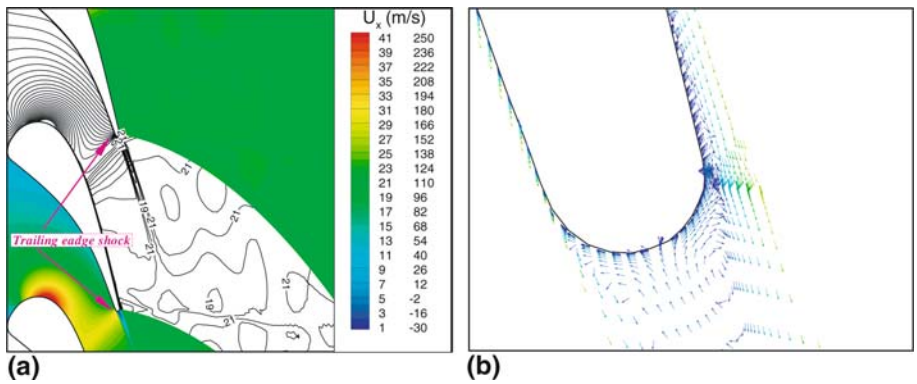

Fig. 8 Simulated axial velocity contours (**a**), velocity vectors (**b**) for the $M_{2,\mathrm{is}} = 1.10$ case

The simulations were run on a HEWLETT-PACKARD KAYAK XU800 machine. A typical running cost for the calculation of the high-exit-Mach-number case, $M_{2,\mathrm{is}} = 1.10$, is about 180 min per elapsed time. The maximum residual reduced by four to five orders of magnitude can generally be achieved after 5,000 iterations.

5 Conclusions

An efficient numerical method, the modified implicit flux-vector-splitting solver (MIFVS), has been extended to solve the transonic-flow problem in highly loaded turbine blades. A compressible low-Reynolds-number k–ε turbulence model and transition model have been implemented into the MIFVS solver.

This extended MIFVS method was then utilized and demonstrated to be numerically efficient and accurate for solving transonic cascade flows through extensive comparisons with the highly loaded VKI guide-vane cascade. Results obtained for the surface pressure, the wake profile and the flow structure show good agreement with the experimental data and other published numerical results. The main features, such as shock/boundary-layer interactions and flow separation, are accurately predicted.

Fig. 9 Simulated contours of density gradient magnitude (numerical Schlieren) for the $M_{2,\mathrm{is}} = 1.10$ case

Further developments are to generalize and validate the present numerical approach to simulations in three space dimensions, with the ultimate goal to routinely apply these to the design and performance analysis of highly loaded turbine blades with great confidence.

Acknowledgements Professor Peter R. Voke, Dr Robert W. Field and Professor Mark A.F. Kendall are acknowledged for their technical insights and discussions.

References

1. Curtis EM, Hodson HP, Banieghbal MR, Denton JD, Howell RJ, Harvey NW (1996) Development of blade profiles for low pressure turbine applications. ASME J Turbomach 119(3):531–538
2. Chima RV (1996) Application of the k-omega turbulence model to quasi-three-dimensional turbomachinery flows. J Propulsion Power 12(6):1176–1179
3. Gehrer A, Jericha H (1998) External heat transfer predictions in a highly-loaded transonic linear turbine guide vane cascade using an upwind biased Navier–Stokes solver. ASME Paper 98-GT-238
4. Hall U, Larsson J, Bario F, Kulisa P, Slimani J, Begin V, Eriksson L-E, Wahlen U (1998) Simulations and measurements on impulse blades for heat transfer prediction in supersonic turbine applications. ASME 98-GT-154, International Gas Turbine & Aeroengine Congress & Exhibition, Stockholm, Sweden
5. Howell RJ, Hodson HP, Schulte V, Stieger RD, Heinz-Peter S, Hasslebach F, Harvey NW (2002) Layer development in the BR710 and BR715 LP turbines—the implementation of high lift and ultra high lift concepts. J Turbomach 124(3):385–392
6. Sarkar S (2005) Wake-induced transitional flow over a highly-loaded LP turbine blade, ASME-GT-2005-68895, ASME Turbo Expo 2005, Reno-Tahoe, Nevada, USA
7. Liu Y, Liu B, Xiang YM (1996) A new highly efficient and accurate implicit flux vector splitting schemes. Chin Sci Bull 41(14):1229–1232
8. Liu Y, Kendall MAF (2004) Numerical simulation of heat transfer from a transonic jet impinging on skin for needle-free powdered drug and vaccine delivery. Proc Inst Mech Eng, Part C: J Mech Eng Sci 218(11):1373–1383
9. Liu Y, Zhang Q (2006) The implicit formulation of flux-vector-splitting scheme with application to transonic flows. Int J Mech Sci 48(11):1208–1222
10. Arts T, Lambert de Rouvroit M, Rutherford AW (1990) Aero-thermal investigation of a highly loaded transonic linear turbine guide vane cascade. VKI Technical Note 174, von Karman Institute for Fluid Dynamics, Belgium
11. Arts T (1994) Highly loaded transonic and film cooed linear turbine guide vane cascade. VKI Lecture series,1994-06, von Karman Institute for Fluid Dynamics, Belgium

12. Liu Y, Bellhouse BJ (2005) Prediction of jet flows in the supersonic nozzle and diffuser. Int J Num Meth Fluids 47:1147–1155
13. Liu Y, Kendall MAF (2007) Simulations of transonic shock-tube flow with a model micro-cylinder in the driver. Comput Meth Programs Biomed 85(2):124–128
14. Chien KY (1982) Predictions of channel and boundary-layer flows with lower-Reynolds-number turbulence model. AIAA J 20(1):33–38
15. Sarkar S, Erlebacher G, Hussaini MY, Kreiss HO (1991) The analysis and modelling of dilational terms in compressible turbulence. J Fluid Mech 227:473–493
16. Cho N-H, Liu X, Rodi W, Schonung B (1993) Calculation of wake-induced unsteady flow in a turbine cascade. ASME J Turbomach 115:675–686
17. Michelassi V, Rodi W (1997) Experimental and numerical investigation of boundary-layer and wake development in a transonic turbine cascade. ASME 97-GT-483. International Gas Turbine & Aeroengine Congress & Exposition, Orlando, FL, USA
18. Kato M, Launder BE (1993) The modelling of turbulent flow around stationary and vibrating square cylinder. Proceedings of 9th symposium on turbulent shere flows, Kyoto, Japan, pp 10.4.1–10.4.6
19. Beam RM, Warming RF (1978) An implicit factored scheme for the compressible Navier–Stokes equations. AIAA J 16(4):393–402
20. Steger JL, Warming RF (1981) Flux vector splitting of the inviscid gasdynamic equations with application to finite-difference methods. J Comput Phys 40:263–293
21. Fluent user's guide volume, Fluent inc., Lebanon, NH 03766, USA. also see Http://www.fluent.com/